

PAPER • OPEN ACCESS

Internal field analysis for scattering of electrically small multilayer spherical scatterers

To cite this article: Arash Nassajy 2025 *J. Opt.* **27** 125601

View the [article online](#) for updates and enhancements.

You may also like

- [Electromagnetic response of nanoparticles with a metallic core and a semiconductor shell](#)

Fahime Seyedheydari, Kevin M Conley, Vaibhav Thakore et al.

- [Anisotropic complex permittivity measurement using a microstrip air line](#)

Qunying Li and Changying Wu

- [Dielectric metal/metal oxide nanocomposites: modeling response properties at multiple scales](#)

Brett Henderson, Archita N S Adluri, Jeffrey T Paci et al.

Internal field analysis for scattering of electrically small multilayer spherical scatterers

Arash Nassajy* 

Faculty of Information Technology and Communication Sciences, Tampere University, 33720 Tampere, Finland

E-mail: arash.nassajy@tuni.fi

Received 7 August 2025, revised 7 November 2025

Accepted for publication 1 December 2025

Published 12 December 2025



CrossMark

Abstract

The Mie theory provides a general electrodynamic method for calculating the scattering coefficients of the internal electric and magnetic fields induced in a multilayer spherical scatterer. Moreover, the use of Taylor and Padé expansion methods paves the way for physically interpretable mathematical forms of the Mie scattering coefficients. This study utilizes the Taylor approximation method along with the idea of equivalent core and ambient permittivities to reformulate the Mie coefficients for induced internal electromagnetic fields of electrically small multilayer spherical scatterers. The procedure begins with a typical triple-layer scatterer, and the formalism is further generalized to express induced fields for an M -layer scatterer. The equivalent core and ambient permittivities let acquisition of new perspective on the subject of internal fields induction, and make it easier to synthesize inclusions with unconventional electromagnetic properties. The deep distinction between equivalent core and ambient permittivities is revealed through further illustration of their variations for a typical quadruple-layered structure.

Keywords: Mie scattering, metamaterials, metasurfaces, surface plasmon polaritons

1. Introduction

The scattering problem for plane electromagnetic waves incident on an isotropic homogeneous spherical particle is commonly known as the Mie theory (which is sometimes called the Lorentz–Mie theory or Lorentz–Mie–Debye theory for historical reasons [1]). The analysis extends to the two concentric spheres in [2] based on the Mie theory. In their work, the boundary conditions at the interfaces of the spherical layers

determine the Mie scattering coefficients. Thus, the theory can be further extended to multilayered spheres by appropriately applying interfacial boundary conditions, and evaluating the determinantal form of the scattering coefficients.

However, some mathematical methods have been developed to circumvent the necessity of inverting ultra-large matrices in the calculation of scattering coefficients. One such early method utilizes logarithmic derivatives and ratios of Riccati–Bessel functions for a single sphere [3]. A similar methodology is used for two concentric spherical nanoparticles [4], and is further expanded to include the analysis of multilayer spherical structures [5]. In fact, a complete set of Mie scattering coefficients is proposed in [5] for the fields within the various regions of an inhomogeneous sphere by obtaining the coefficients of an m -layered sphere from those of an $(m-1)$ -layered sphere in a recursive manner.

* Author to whom any correspondence should be addressed.



Original content from this work may be used under the terms of the [Creative Commons Attribution 4.0 licence](https://creativecommons.org/licenses/by/4.0/). Any further distribution of this work must maintain attribution to the author(s) and the title of the work, journal citation and DOI.

Despite a concise recurrence formula, numerical problems and computational difficulties are still encountered for scatterers with thin spherical shells, strongly absorbing complex media, and a large number of concentric layers [6]. These problems leads to a widely studied research topic in the literature with the expectation of proposing novel computational algorithms for the improvement of previously developed methods in terms of extended ranges of applicability. Consequently, a stable and accurate iterative method for any complex refractive indices regardless of the size of the particle is presented in [7]. This work is extended in [8] in slightly modified form to include the calculation of the internal field. An improvement that uses the Taylor expansion for the ratios of the Riccati–Bessel function is proposed in [9] to overcome the round-off errors; although, it is claimed by [10] that such a Taylor expansion is not required if a modified algorithm is used. A more concise and numerically stable algorithm to overcome the numerical inaccuracies of other methods is presented by [11]. The algorithm presented in [11] is the basis upon which some computer programs are implemented both for far-field [12] and near-field electromagnetic radiation [13].

In addition to recursive algorithms, the transfer matrix formalism is used to address the scattering problem of electromagnetic waves in multilayered spheres [14]. The limits of the methods mentioned in the previous paragraph for thin complex shells are overcome by combining recursive methods with the transfer matrix method [6]. A progressive algorithm is also reported that permits the calculation of the scattering coefficients for a selected internal layer without the necessity of evaluating the coefficients for all other layers [15]. Although all these methods mentioned so far are proposed to express Mie scattering coefficients in a rigorous and simple way, they do not provide us with the physical insight required to practically interpret scattering phenomena.

An early physical technique is presented in [16] that draws an analogy between scattering from radially inhomogeneous sphere and non-uniform transmission line theory. Same analogy is investigated in [17] by the use of electrostatic analysis. In this analysis, the Laplace equation is solved instead of the wave equation in the first place. Although the electrostatic approach allows the interpretation of mixtures in terms of polarizability and effective permittivity [18, 19], it lacks the complete electrodynamics perspective that can be achieved by Mie theory.

The lack of physical insight in Mie scattering coefficients can be compensated for by approximation techniques that offer physically interpretable mathematical forms of Mie scattering coefficients. In fact, for electrically small or subwavelength particles, the quasistatic analysis is valid, in which the Taylor expansion of Mie scattering coefficients are calculated [20–26]. The Taylor approximation reveals the plasmonic multipole resonances and the possibility for the occurrence of phenomena like localized surface plasmonic resonances (LSPR). The electrostatic technique merely offers the dipole resonance; although, the quasistatic analysis also shows that the higher

modes (quadrupole, etc) are dramatically suppressed in front of the dominant dipole mode for subwavelength nanoparticles.

For electrically large scatterers, the higher order multipoles are present and size-dependent resonating aspects like a self-regulating radiative damping mechanism and the dynamic depolarization are observable. These electrodynamic effects along with anomalous resonances (Fano-like resonances) are recently interpreted via the Padé expansion of the Mie scattering coefficients [27–30].

The analysis of electromagnetic wave scattering from spherical scatterer is a canonical problem, and the methods mentioned so far construct a complete solution. However, new insight might be obtained by the reformulation of the aforementioned techniques. In this way, it is proposed in [31–33] that an electrically small multilayer scatterer can be identified as a single-layer spherical scatterer with an equivalent permittivity.

This study re-expresses the solutions of the internal electromagnetic fields for an electrically small multilayered spherical scatterer induced from an incident plane wave. This re-expression is achieved based on the equivalent permittivities. In fact, the idea of equivalent core permittivity mentioned in the last paragraph is extended to an analogous idea of equivalent ambient permittivity. Section 2 presents the formulae of induced internal fields, and the reformulation by equivalent permittivities is presented in section 3. A comparison between the equivalent core and ambient permittivities is illustrated in section 4, and new insight readily available from the reformulated expressions is offered for some cases in section 5. The time convention $e^{i\omega t}$ is assumed throughout.

2. Induced field analysis

The electric and magnetic fields that are induced in a spherical structure by an incident plane wave can be evaluated by decomposing the impinging wave into sets of vector spherical wave functions (VSWFs) [2, 34]. For a monochromatic plane wave propagating in the positive z direction with its electric field linearly polarized in the x direction ($\mathbf{E}_i = E_0 e^{-ik_a z} \hat{\mathbf{x}}$; k_a is the wave number of the ambient, and E_0 is the complex electric field amplitude), the induced electric and magnetic fields in the m th layer of a multilayered spherical scatterer can be expanded as [26]:

$$\begin{aligned} \mathbf{E}_m &= \sum_{n=1}^{\infty} E_n \left(a_n^{(m)} \mathbf{m}_n^{oh} + b_n^{(m)} \mathbf{m}_n^{oj} + ic_n^{(m)} \mathbf{n}_n^{eh} + id_n^{(m)} \mathbf{n}_n^{ej} \right), \\ \mathbf{H}_m &= \sum_{n=1}^{\infty} \frac{iE_n}{\eta_m} \left(a_n^{(m)} \mathbf{n}_n^{oh} + b_n^{(m)} \mathbf{n}_n^{oj} + ic_n^{(m)} \mathbf{m}_n^{eh} + id_n^{(m)} \mathbf{m}_n^{ej} \right), \end{aligned} \quad (1)$$

where $E_n = E_0 (-i)^n \frac{2n+1}{n(n+1)}$, and η_m is the characteristic impedance of the m th layer. The $a_n^{(m)}$, $b_n^{(m)}$, $c_n^{(m)}$, and $d_n^{(m)}$ are Mie expansion coefficients for the m th layer, and \mathbf{m}_n^{oh} , \mathbf{m}_n^{oj} , \mathbf{n}_n^{eh} , \mathbf{n}_n^{ej}

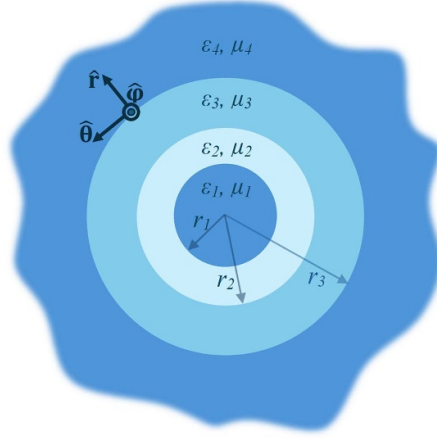


Figure 1. The cross section of a triple-layered spherical scatterer centered at the origin of a spherical coordinate system (r, θ, ϕ) .

\mathbf{m}_n^{oh} , \mathbf{m}_n^{eh} , \mathbf{n}_n^{oh} , and \mathbf{n}_n^{eh} are VSWFs defined as below:

$$\mathbf{m}_n^{oj} = j_n(k_m r) \frac{P_n^1(\cos\theta)}{\sin\theta} \cos\phi \hat{\boldsymbol{\theta}} - j_n(k_m r) \frac{d}{d\theta} P_n^1(\cos\theta) \sin\phi \hat{\boldsymbol{\phi}}, \quad (2a)$$

$$\mathbf{m}_n^{ej} = -j_n(k_m r) \frac{P_n^1(\cos\theta)}{\sin\theta} \sin\phi \hat{\boldsymbol{\theta}} - j_n(k_m r) \frac{d}{d\theta} P_n^1(\cos\theta) \cos\phi \hat{\boldsymbol{\phi}}, \quad (2b)$$

$$\mathbf{n}_n^{oj} = n(n+1) \frac{j_n(k_m r)}{k_m r} P_n^1(\cos\theta) \sin\phi \hat{\mathbf{r}} + \frac{[k_m r j_n(k_m r)]'}{k_m r} \frac{d}{d\theta} P_n^1(\cos\theta) \sin\phi \hat{\boldsymbol{\theta}} + \frac{[k_m r j_n(k_m r)]'}{k_m r} \frac{P_n^1(\cos\theta)}{\sin\theta} \cos\phi \hat{\boldsymbol{\phi}}, \quad (2c)$$

$$\mathbf{n}_n^{ej} = n(n+1) \frac{j_n(k_m r)}{k_m r} P_n^1(\cos\theta) \cos\phi \hat{\mathbf{r}} + \frac{[k_m r j_n(k_m r)]'}{k_m r} \frac{d}{d\theta} P_n^1(\cos\theta) \cos\phi \hat{\boldsymbol{\theta}} - \frac{[k_m r j_n(k_m r)]'}{k_m r} \frac{P_n^1(\cos\theta)}{\sin\theta} \sin\phi \hat{\boldsymbol{\phi}}. \quad (2d)$$

In (2), $j_n(\cdot)$ is the spherical Bessel function of the first kind and the n th order, and the derivative is in respect to the argument $k_m r$. P_n^1 is the associated Legendre polynomial of the first kind, the first order and the n th degree. The \mathbf{m}_n^{oh} , \mathbf{m}_n^{eh} , \mathbf{n}_n^{oh} , and \mathbf{n}_n^{eh} can be defined with the same expressions of (2) except that $j_n(\cdot)$ is replaced with $h_n^{(2)}(\cdot)$, the spherical Hankel function of the second kind and the n th order. The $h_n^{(2)}(\cdot)$ is defined as $h_n^{(2)}(\cdot) = j_n(\cdot) - i y_n(\cdot)$, where $y_n(\cdot)$ is the spherical Bessel function of the second kind and the n th order.

In the layer indexing, the core and the ambient are considered as layers in a spherically stratified space. Each layer

has inner radius r_{m-1} and outer radius r_m , and is specified by isotropic homogeneous materials with permittivity ε_m and permeability μ_m at operating frequency ω . The materials are considered lossless or low-loss with $\text{Im}(\varepsilon_m) \ll |\text{Re}(\varepsilon_m)|$ and $\text{Im}(\mu_m) \ll |\text{Re}(\mu_m)|$.

The expansion coefficients $(a_n^{(m)}, b_n^{(m)}, c_n^{(m)}, \text{ and } d_n^{(m)})$ are determined by the boundary conditions at the discontinuities of adjacent regions (for $m = 1, \dots, M$) and by the necessary conditions for the fields to be meaningful both at the origin and the infinity. Thus, $a_n^{(1)} = c_n^{(1)} = 0$ and $b_n^{(M)} = d_n^{(M)} = 0$.

Here, only the induced fields in the core and the concentric layers are of concern ($m = 1, \dots, M - 1$). Also, the following analysis is limited to the TM^r polarization ($c_n^{(m)}$ and $d_n^{(m)}$), and similar expressions can be obtained for TE^r-polarized field ($a_n^{(m)}$ and $b_n^{(m)}$ respectively) by replacing ε with μ in all the equations that follows.

Let us start with a triple-layered scatterer shown in figure 1. The Mie scattering coefficients for each layer can be written as follows:

$$c_n^{(1)} = 0, \quad d_n^{(1)} = -i \frac{V_n^{(1)}}{U_n^{(4)}} \frac{V_n^{(4)}}{1 - i \frac{V_n^{(4)}}{U_n^{(4)}}}, \quad (3a)$$

$$c_n^{(2)} = -\frac{U_n^{(2)}}{U_n^{(4)}} \frac{V_n^{(4)}}{1 - i \frac{V_n^{(4)}}{U_n^{(4)}}}, \quad d_n^{(2)} = -c_n^{(2)} - i \frac{U_n^{(2)}}{U_n^{(4)}} \frac{V_n^{(4)}}{1 - i \frac{V_n^{(4)}}{U_n^{(4)}}}, \quad (3b)$$

$$c_n^{(3)} = \frac{U_n^{(3)}}{U_n^{(4)}} \frac{V_n^{(4)}}{1 - i \frac{V_n^{(4)}}{U_n^{(4)}}}, \quad d_n^{(3)} = -c_n^{(3)} + i \frac{U_n^{(3)}}{U_n^{(4)}} \frac{V_n^{(4)}}{1 - i \frac{V_n^{(4)}}{U_n^{(4)}}}, \quad (3c)$$

where $V_n^{(1)}, V_n^{(2)}, V_n^{(3)}, V_n^{(4)}, U_n^{(2)}, U_n^{(3)}, \text{ and } U_n^{(4)}$ are determinants of 6×6 matrices. $V_n^{(1)}, U_n^{(2)}, U_n^{(3)}, \text{ and } U_n^{(4)}$ are expressed as follows:

$$V_n^{(1)} = \begin{pmatrix} j_n(k_2r_1) & y_n(k_2r_1) & 0 & 0 & 0 & 0 \\ \frac{[k_2r_1j_n(k_2r_1)]'}{\varepsilon_2} & \frac{[k_2r_1y_n(k_2r_1)]'}{\varepsilon_2} & 0 & 0 & 0 & 0 \\ j_n(k_2r_2) & y_n(k_2r_2) & j_n(k_3r_2) & y_n(k_3r_2) & 0 & 0 \\ \frac{[k_2r_2j_n(k_2r_2)]'}{\varepsilon_2} & \frac{[k_2r_2y_n(k_2r_2)]'}{\varepsilon_2} & \frac{[k_3r_2j_n(k_3r_2)]'}{\varepsilon_3} & \frac{[k_3r_2y_n(k_3r_2)]'}{\varepsilon_3} & 0 & 0 \\ 0 & 0 & j_n(k_3r_3) & y_n(k_3r_3) & j_n(k_4r_3) & y_n(k_4r_3) \\ 0 & 0 & \frac{[k_3r_3j_n(k_3r_3)]'}{\varepsilon_3} & \frac{[k_3r_3y_n(k_3r_3)]'}{\varepsilon_3} & \frac{[k_4r_3j_n(k_4r_3)]'}{\varepsilon_4} & \frac{[k_4r_3y_n(k_4r_3)]'}{\varepsilon_4} \end{pmatrix}, \quad (4)$$

$$U_n^{(2)} = \begin{pmatrix} j_n(k_1r_1) & j_n(k_2r_1) & 0 & 0 & 0 & 0 \\ \frac{[k_1r_1j_n(k_1r_1)]'}{\varepsilon_1} & \frac{[k_2r_1j_n(k_2r_1)]'}{\varepsilon_2} & 0 & 0 & 0 & 0 \\ 0 & j_n(k_2r_2) & j_n(k_3r_2) & y_n(k_3r_2) & 0 & 0 \\ 0 & \frac{[k_2r_2j_n(k_2r_2)]'}{\varepsilon_2} & \frac{[k_3r_2j_n(k_3r_2)]'}{\varepsilon_3} & \frac{[k_3r_2y_n(k_3r_2)]'}{\varepsilon_3} & 0 & 0 \\ 0 & 0 & j_n(k_3r_3) & y_n(k_3r_3) & j_n(k_4r_3) & y_n(k_4r_3) \\ 0 & 0 & \frac{[k_3r_3j_n(k_3r_3)]'}{\varepsilon_3} & \frac{[k_3r_3y_n(k_3r_3)]'}{\varepsilon_3} & \frac{[k_4r_3j_n(k_4r_3)]'}{\varepsilon_4} & \frac{[k_4r_3y_n(k_4r_3)]'}{\varepsilon_4} \end{pmatrix}, \quad (5)$$

$$U_n^{(3)} = \begin{pmatrix} j_n(k_1r_1) & j_n(k_2r_1) & y_n(k_2r_1) & 0 & 0 & 0 \\ \frac{[k_1r_1j_n(k_1r_1)]'}{\varepsilon_1} & \frac{[k_2r_1j_n(k_2r_1)]'}{\varepsilon_2} & \frac{[k_2r_1y_n(k_2r_1)]'}{\varepsilon_2} & 0 & 0 & 0 \\ 0 & j_n(k_2r_2) & y_n(k_2r_2) & j_n(k_3r_2) & 0 & 0 \\ 0 & \frac{[k_2r_2j_n(k_2r_2)]'}{\varepsilon_2} & \frac{[k_2r_2y_n(k_2r_2)]'}{\varepsilon_2} & \frac{[k_3r_2j_n(k_3r_2)]'}{\varepsilon_3} & 0 & 0 \\ 0 & 0 & 0 & j_n(k_3r_3) & j_n(k_4r_3) & y_n(k_4r_3) \\ 0 & 0 & 0 & \frac{[k_3r_3j_n(k_3r_3)]'}{\varepsilon_3} & \frac{[k_4r_3j_n(k_4r_3)]'}{\varepsilon_4} & \frac{[k_4r_3y_n(k_4r_3)]'}{\varepsilon_4} \end{pmatrix}, \quad (6)$$

$$U_n^{(4)} = \begin{pmatrix} j_n(k_1r_1) & j_n(k_2r_1) & y_n(k_2r_1) & 0 & 0 & 0 \\ \frac{[k_1r_1j_n(k_1r_1)]'}{\varepsilon_1} & \frac{[k_2r_1j_n(k_2r_1)]'}{\varepsilon_2} & \frac{[k_2r_1y_n(k_2r_1)]'}{\varepsilon_2} & 0 & 0 & 0 \\ 0 & j_n(k_2r_2) & y_n(k_2r_2) & j_n(k_3r_2) & y_n(k_3r_2) & 0 \\ 0 & \frac{[k_2r_2j_n(k_2r_2)]'}{\varepsilon_2} & \frac{[k_2r_2y_n(k_2r_2)]'}{\varepsilon_2} & \frac{[k_3r_2j_n(k_3r_2)]'}{\varepsilon_3} & \frac{[k_3r_2y_n(k_3r_2)]'}{\varepsilon_3} & 0 \\ 0 & 0 & 0 & j_n(k_3r_3) & y_n(k_3r_3) & j_n(k_4r_3) \\ 0 & 0 & 0 & \frac{[k_3r_3j_n(k_3r_3)]'}{\varepsilon_3} & \frac{[k_3r_3y_n(k_3r_3)]'}{\varepsilon_3} & \frac{[k_4r_3j_n(k_4r_3)]'}{\varepsilon_4} \end{pmatrix}. \quad (7)$$

$V_n^{(2)}$, $V_n^{(3)}$, and $V_n^{(4)}$ can be obtained from $U_n^{(2)}$, $U_n^{(3)}$, and $U_n^{(4)}$, respectively, by replacing $j_n(\cdot)$ with $y_n(\cdot)$ in the second column of $U_n^{(2)}$, in the fourth column of $U_n^{(3)}$, and in the sixth column of $U_n^{(4)}$. The difference between the signs of (3b) and (3c) is sourced from the fact that the determinants in (3) are defined so that the columns with the constitutive parameters of the innermost layers come first.

3. Electrically small scatterer

For electrically small scatterer, one can use the approximate expressions for the Bessel functions (see appendix IV in [35]). $U_n^{(4)}$ is written with these approximated forms as follows:

$$U_n^{(4)} = j_n(k_1 r_1) j_n(k_4 r_3) \prod_{m=2}^3 j_n(k_m r_{m-1}) y_n(k_m r_{m-1})$$

$$\times \begin{vmatrix} 1 & 1 & 1 & 0 & 0 & 0 \\ \frac{n+1}{\varepsilon_1} & \frac{n+1}{\varepsilon_2} & -\frac{n}{\varepsilon_2} & 0 & 0 & 0 \\ 0 & \gamma_2^{-n} & \gamma_2^{n+1} & 1 & 1 & 0 \\ 0 & \frac{n+1}{\varepsilon_2} \gamma_2^{-n} & -\frac{n}{\varepsilon_2} \gamma_2^{n+1} & \frac{n+1}{\varepsilon_3} & -\frac{n}{\varepsilon_3} & 0 \\ 0 & 0 & 0 & \gamma_3^{-n} & \gamma_3^{n+1} & 1 \\ 0 & 0 & 0 & \frac{n+1}{\varepsilon_3} \gamma_3^{-n} & -\frac{n}{\varepsilon_3} \gamma_3^{n+1} & \frac{n+1}{\varepsilon_4} \end{vmatrix}, \quad (8)$$

in which $\gamma_m \equiv \frac{r_{m-1}}{r_m}$. It should be noted that the Bessel functions are rewritten in their closed form after using the approximation to save the space in (8). All the other determinants used in (3) can be obtained in a similar manner. These approximated forms are utilized to derive the determinant ratios in (3). After evaluating $V_n^{(4)}$ and $U_n^{(4)}$, the ratio $\frac{V_n^{(4)}}{U_n^{(4)}}$ can be rewritten by the idea of equivalent core permittivity as follows:

$$\frac{V_n^{(4)}}{U_n^{(4)}} = \frac{y_n(k_4 r_3)}{j_n(k_4 r_3)} \frac{n\varepsilon_c^{(4)} + (n+1)\varepsilon_4}{(n+1)[\varepsilon_c^{(4)} - \varepsilon_4]}, \quad (9)$$

where $\varepsilon_c^{(4)}$ is the equivalent core permittivity that the fourth layer (ambient region) sees, and $\varepsilon_c^{(m)}$, in general, is obtained from the following recursive formula:

$$\varepsilon_c^{(m)} = \frac{1 + (n+1)\Gamma_c^{(m-1)}}{1 - n\Gamma_c^{(m-1)}} \varepsilon_{m-1}, \quad (10)$$

where

$$\Gamma_c^{(m)} = \frac{\varepsilon_c^{(m)} - \varepsilon_m}{n\varepsilon_c^{(m)} + (n+1)\varepsilon_m} \gamma_m^{2n+1}. \quad (11)$$

It is assumed that $\Gamma_c^{(1)} = 0$ to make the foregoing recurrence relation consistent. The relations for the other determinant ratios in (3) are expressed as follows for each layer:

$$\frac{U_n^{(3)}}{U_n^{(4)}} = \frac{y_n(k_4 r_3)}{y_n(k_3 r_2)} \cdot \frac{-(2n+1)\gamma_3^n \varepsilon_3}{[(n+1)\varepsilon_3 + n\varepsilon_4]\gamma_3^{2n+1} + \frac{n\varepsilon_c^{(3)} + (n+1)\varepsilon_3}{[\varepsilon_c^{(3)} - \varepsilon_3]} [\varepsilon_3 - \varepsilon_4]}, \quad (12a)$$

$$\frac{V_n^{(3)}}{U_n^{(4)}} = \frac{y_n(k_4 r_3)}{j_n(k_3 r_2)} \cdot \frac{n\varepsilon_c^{(3)} + (n+1)\varepsilon_3}{(n+1)[\varepsilon_c^{(3)} - \varepsilon_3]} \cdot \frac{(2n+1)\gamma_3^n \varepsilon_3}{[(n+1)\varepsilon_3 + n\varepsilon_4]\gamma_3^{2n+1} + \frac{n\varepsilon_c^{(3)} + (n+1)\varepsilon_3}{[\varepsilon_c^{(3)} - \varepsilon_3]} [\varepsilon_3 - \varepsilon_4]}, \quad (12b)$$

$$\frac{U_n^{(2)}}{U_n^{(4)}} = \frac{y_n(k_4 r_3)}{y_n(k_2 r_1)} \cdot \frac{(2n+1)\gamma_2^n \varepsilon_2}{\left[(n+1)\varepsilon_2 + n\varepsilon_a^{(2)} \right] \gamma_2^{2n+1} + \frac{n\varepsilon_1 + (n+1)\varepsilon_2}{[\varepsilon_1 - \varepsilon_2]} [\varepsilon_2 - \varepsilon_a^{(2)}]} \cdot \frac{(2n+1)\gamma_3^n \varepsilon_3}{[(n+1)\varepsilon_3 + n\varepsilon_4]\gamma_3^{2n+1} + n[\varepsilon_3 - \varepsilon_4]}, \quad (13a)$$

$$\frac{V_n^{(2)}}{U_n^{(4)}} = \frac{y_n(k_4 r_3)}{j_n(k_2 r_1)} \cdot \frac{n\varepsilon_1 + (n+1)\varepsilon_2}{(n+1)[\varepsilon_1 - \varepsilon_2]} \cdot \frac{-(2n+1)\gamma_2^n \varepsilon_2}{\left[(n+1)\varepsilon_2 + n\varepsilon_a^{(2)} \right] \gamma_2^{2n+1} + \frac{n\varepsilon_1 + (n+1)\varepsilon_2}{[\varepsilon_1 - \varepsilon_2]} [\varepsilon_2 - \varepsilon_a^{(2)}]} \cdot \frac{(2n+1)\gamma_3^n \varepsilon_3}{[(n+1)\varepsilon_3 + n\varepsilon_4]\gamma_3^{2n+1} + n[\varepsilon_3 - \varepsilon_4]}, \quad (13b)$$

$$\frac{V_n^{(1)}}{U_n^{(4)}} = \frac{y_n(k_4 r_3)}{j_n(k_1 r_1)} \cdot \frac{-(2n+1)\varepsilon_1}{(n+1)[\varepsilon_1 - \varepsilon_a^{(1)}]} \cdot \frac{(2n+1)\gamma_2^n \varepsilon_2}{\left[(n+1)\varepsilon_2 + n\varepsilon_a^{(2)} \right] \gamma_2^{2n+1} + n[\varepsilon_2 - \varepsilon_a^{(2)}]} \cdot \frac{(2n+1)\gamma_3^n \varepsilon_3}{[(n+1)\varepsilon_3 + n\varepsilon_4]\gamma_3^{2n+1} + n[\varepsilon_3 - \varepsilon_4]}. \quad (14)$$

Note that the analogous idea of equivalent ambient permittivity ($\varepsilon_a^{(m)}$) is utilized to reformulate the relations in (13) and (14). The $\varepsilon_a^{(m)}$ is the equivalent ambient permittivity that the m th layer sees and is expressed as follows:

$$\varepsilon_a^{(m)} = \frac{1 + (n+1)\Gamma_a^{(m+1)}}{1 - n\Gamma_a^{(m+1)}} \varepsilon_{m+1}, \quad (15)$$

where

$$\Gamma_a^{(m)} = \frac{\varepsilon_a^{(m)} - \varepsilon_m}{n\varepsilon_a^{(m)} + (n+1)\varepsilon_m} \gamma_m^{-2n-1}. \quad (16)$$

For consistency, it is again presumed that $\Gamma_a^{(M)} = 0$. It is noteworthy that $\varepsilon_a^{(3)}$ is simply replaced with ε_4 in (12)–(14). In the same manner, ε_1 replaces $\varepsilon_c^{(2)}$ in (13). Next section compares the equivalent core and ambient permittivities.

The inspection of (12) shows that negative signs arise in $\frac{U_n^{(3)}}{U_n^{(4)}}$ and $\frac{V_n^{(3)}}{U_n^{(4)}}$ in contrast with $\frac{U_n^{(2)}}{U_n^{(4)}}$ and $\frac{V_n^{(2)}}{U_n^{(4)}}$ in (13), respectively. By considering these negative signs, coherent forms of $c_n^{(m)}$ and $d_n^{(m)}$ are revealed as follows for an M -layer subwavelength scatterer:

$$c_n^{(1)} = 0, \quad d_n^{(1)} = -i \frac{V_n^{(1)}}{U_n^{(M)}} \frac{1}{1 - i \frac{V_n^{(M)}}{U_n^{(M)}}}, \quad (17a)$$

$$c_n^{(m)} = -\frac{U_n^{(m)}}{U_n^{(M)}} \frac{1}{1 - i \frac{V_n^{(M)}}{U_n^{(M)}}}, \quad d_n^{(m)} = -c_n^{(m)} - i \frac{V_n^{(m)}}{U_n^{(M)}} \frac{1}{1 - i \frac{V_n^{(M)}}{U_n^{(M)}}}, \quad (17b)$$

where the determinant ratios are defined in the next paragraph.

The juxtaposition of (12)–(14) reveals the pattern that by defining the following parameter for the core:

$$\beta_1 = \frac{(2n+1)\varepsilon_1}{(n+1)[\varepsilon_1 - \varepsilon_a^{(1)}]}, \quad (18)$$

and the following parameters for the concentric layers:

$$\alpha_m = \frac{n\varepsilon_c^{(m)} + (n+1)\varepsilon_m}{\varepsilon_c^{(m)} - \varepsilon_m}, \quad (19)$$

$$\beta_m = \frac{(2n+1)\gamma_m^n \varepsilon_m}{[(n+1)\varepsilon_m + n\varepsilon_a^{(m)}]\gamma_m^{2n+1} + n[\varepsilon_m - \varepsilon_a^{(m)}]}, \quad (20)$$

$$\beta_m^\alpha = \frac{(2n+1)\gamma_m^n \varepsilon_m}{[(n+1)\varepsilon_m + n\varepsilon_a^{(m)}]\gamma_m^{2n+1} + \alpha_m[\varepsilon_m - \varepsilon_a^{(m)}]}, \quad (21)$$

the determinant ratios in (17) can be compactly written in the following forms:

$$\frac{V_n^{(M)}}{U_n^{(M)}} = \frac{4^n (2n+1) (n - \frac{1}{2})!^2}{\pi (k_M r_{M-1})^{2n+1}} \cdot \frac{n\varepsilon_c^{(M)} + (n+1)\varepsilon_M}{(n+1)[\varepsilon_c^{(M)} - \varepsilon_M]}, \quad (22)$$

$$\frac{U_n^{(m)}}{U_n^{(M)}} = \left(\frac{k_m r_{m-1}}{k_M r_{M-1}}\right)^{n+1} \cdot \beta_m^\alpha \prod_{l=m+1}^{M-1} \beta_l, \quad (23)$$

$$\frac{V_n^{(m)}}{U_n^{(M)}} = \frac{4^n (2n+1) (n - \frac{1}{2})!^2}{\pi (k_M r_{M-1})^{n+1} (k_m r_{m-1})^n} \cdot \frac{\alpha_m \beta_m^\alpha}{n+1} \prod_{l=m+1}^{M-1} \beta_l, \quad (24)$$

$$\frac{V_n^{(1)}}{U_n^{(M)}} = \frac{4^n (2n+1) (n - \frac{1}{2})!^2}{\pi (k_M r_{M-1})^{n+1} (k_1 r_1)^n} \cdot \beta_1 \prod_{l=2}^{M-1} \beta_l. \quad (25)$$

Here, the approximated forms of Bessel functions are used in (22) through (25). Also, it should be noted that, throughout this section, the analysis is proceeded for all values of n for the sake of keeping relations general despite the fact that the

dipole mode dominates [36]. In the following two sections, only the dominant mode ($n = 1$) is of concern.

4. A comparison

The comparison between (10) and (15) reveals that they have the same form except that the expression of $\Gamma_c^{(m)}$ is a function of γ_m^{2n+1} , whereas $\Gamma_a^{(m)}$ is expressed as a function of γ_m^{-2n-1} . The difference that this makes can be demonstrated for the equivalent core and ambient permittivities of the third layer of a quadruple-layered scatterer depicted in figure 2. It is assumed to be equal the permittivities of the core and the ambient region ($\varepsilon_5 = \varepsilon_1$) as well as the permittivities of the second and the fourth layers ($\varepsilon_4 = \varepsilon_2$) for better comparison. Also, as figure 2 shows, it is presumed that $\gamma_2 = \gamma_4 = \gamma$.

The variation of ε_c and ε_a with respect to ε_1 and ε_2 for $\gamma = 0.5$ is shown in figures 3 and 4, respectively. Here, ε_c , ε_a , ε_1 and ε_2 are considered as relative permittivities. As figures 3 and 4 show, the ε_c and ε_a are infinite for some values of ε_1 and ε_2 . This can be better seen from the contour lines of ε_c and ε_a depicted in figure 5 (the values of ε_c and ε_a greater than 25 are cut for better rendering).

The following relation represents the line equation, for which values, ε_c is infinite:

$$\varepsilon_2 = -\frac{n + (n+1)\gamma^{2n+1}}{(n+1)(1 - \gamma^{2n+1})}\varepsilon_1, \quad (26)$$

and the contour lines for specific values of ε_c is obtained from the following quadratic equation:

$$(n+1)(1 - \gamma^{2n+1})\varepsilon_2^2 + [(n + (n+1)\gamma^{2n+1})\varepsilon_1 - ((n+1) + n\gamma^{2n+1})\varepsilon_c]\varepsilon_2 - n(1 - \gamma^{2n+1})\varepsilon_1\varepsilon_c = 0. \quad (27)$$

Similar relations can be obtained for ε_a by replacing γ^{2n+1} with γ^{-2n-1} in (26) and (27).

The contour lines of ε_c and ε_a for $\gamma = 0.2$ are also illustrated in figure 6. One can infer, by comparing figure 5(a) with figure 6(a), that when γ decreases, ε_c changes from being predominantly influenced by ε_1 to being dominated by ε_2 . This seems reasonable when one think of the two extreme cases that happen in a core-shell spherical structure: in the lower limit a thick shell with a very tiny core inside (small γ), and in the higher limit a core with a shell of ultrathin thickness (large γ). In these two extremes, as expected, the constitutive parameters of one layer dominates. The same reasoning is valid for ε_a (figures 5(b) and 6(b)). However, in contrary to ε_c , the values of ε_a are not equal to ε_2 . Note that, for small γ 's, $\varepsilon_c \simeq \varepsilon_2$, but $\varepsilon_a \simeq -2\varepsilon_2$. These results are approved by (10) and (15).

The main difference between ε_c and ε_a is the fact that ε_a can be negative even if ε_1 and ε_2 are both positive. This is shown in figures 5(b) and 6(b). In contrast, one of the ε_1 or ε_2 must be negative in order that ε_c be negative. This counter-intuitive

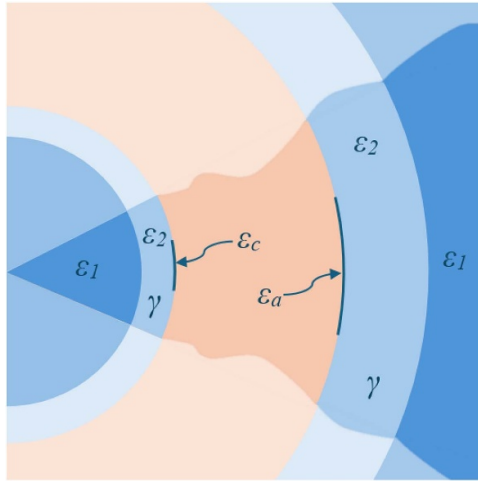


Figure 2. The cross section of a quadruple-layered spherical scatterer.

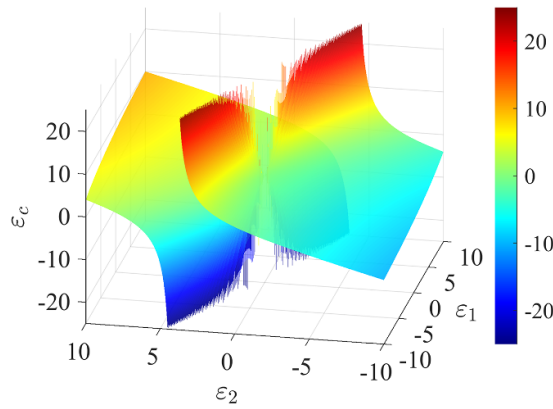


Figure 3. The equivalent core permittivity sketched in figure 2.

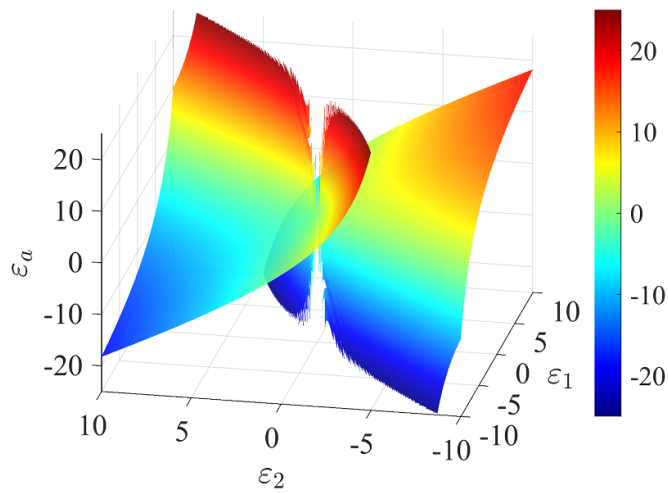


Figure 4. The equivalent ambient permittivity sketched in figure 2.

result can be understood mathematically by noting that (10) and (15) have the same form except for the expressions of $\Gamma_c^{(m)}$ and $\Gamma_a^{(m)}$ as mentioned in the beginning of this section. Since

$\gamma_m^{2n+1} < 1$, $\Gamma_a^{(m)}$ can be greater than unity, which in turn causes $\epsilon_a^{(m)}$ to have the potential to be negative even if all the permittivities are positive.

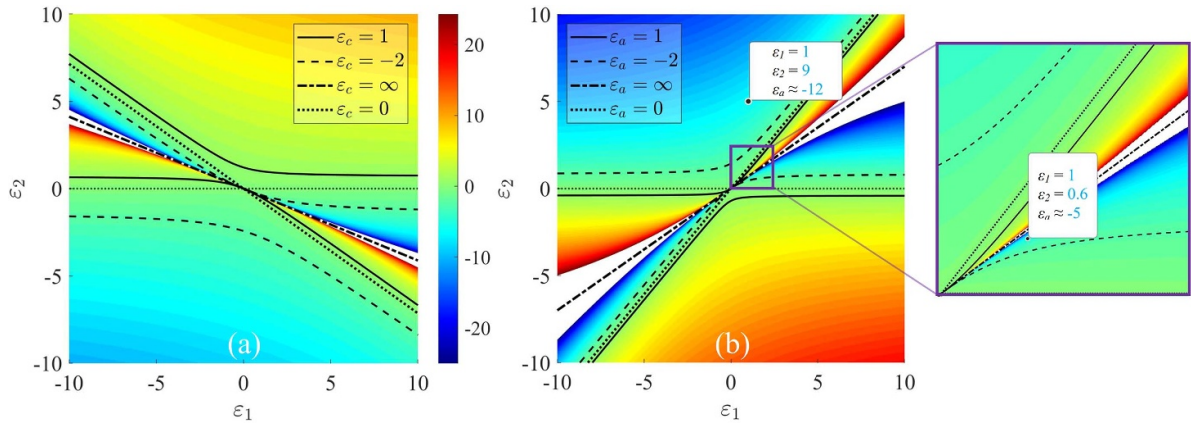


Figure 5. The equivalent (a) core permittivity and (b) ambient permittivity for a fixed $\gamma = 0.5$. The inset figure shows magnification on a region of part (b). (The contour lines greater than 25 are not shown for better rendering; for this reason there is a blank region around the line of infinite values.)

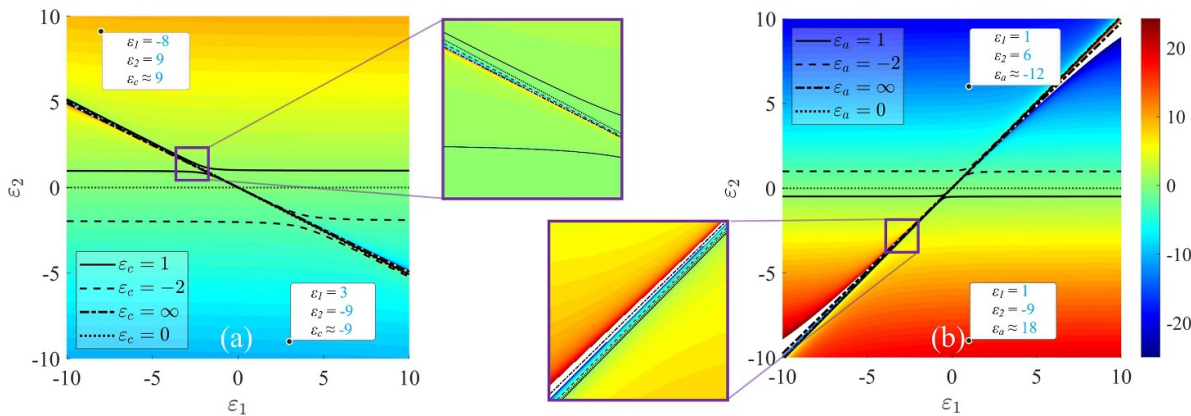


Figure 6. The equivalent (a) core permittivity and (b) ambient permittivity for a fixed $\gamma = 0.2$. The inset figures show magnification on regions of parts (a) and (b). (The contour lines greater than 25 are not shown for better rendering; for this reason there is a blank region around the line of infinite values.)

The physical interpretation of this result can be followed by comparing the directions of the power flux and the propagated wave [37, 38]. Consider a hollow spherical shell made from a material with positive permittivity as the scatterer. Also imagine that two observers are placed one in the interior (S_1) and the other in the exterior (S_2) of the scatterer so that they both are in the regions with permittivities of free space. There is an external excitation in the side of S_2 . Now, the equivalent permittivities that S_1 and S_2 observe (namely ϵ_a and ϵ_c) are essentially different since their perception of free space are not the same: S_1 observes a shell and beyond that shell an infinite free space, while S_2 sees a shell on a spherical free space. That way, the field configurations and the power fluxes are perceived differently by the two different observers, and by considering the fact that the external excitation is in the infinite free space towards S_1 , it can be explained why ϵ_a can be even negative (the direction of the power flux and the field can be different).

The other difference is the applicability of ϵ_c and ϵ_a in calculating the Mie coefficients. It can be seen in (22) through (25) that it is sufficient to know ϵ_c for the m th layer,

but one has to calculate ϵ_a for all layers that comes after the m th layer (including the m th layer itself). This might appear to be a disadvantage and the whole concept of equivalent ambient permittivity to be mere computational aid, but it can have very real physical significance. The next section shows the importance of the reformulations obtained in the previous section to better understanding the mechanism of internal field induction for a electrically small scatterer.

5. Some special cases

Back to the subject of induced internal fields for sub-wavelength nanoparticles, some special cases are considered in this section to demonstrate how the relations obtained in section 3 can be used to acquire new perspective.

Case 1. The further investigation of (17) shows that $c_n^{(m)} = -d_n^{(m)}$ if $\frac{V_n^{(m)}}{U_n^{(m)}} = 0$. In this case, back to (1) and (2), $j_n(k_m r)$ is subtracted from $h_n^{(2)}(k_m r)$ and the electromagnetic fields (E_m and H_m) are functions of $y_n(k_m r)$. This means

that the induced fields in the m th layer are of standing wave type.

For subwavelength scatterer, the fact that the induced field is a standing wave seems irrelevant. Nonetheless, it seems to be of no little importance to check, under what conditions, $\frac{V_n^{(m)}}{U_n^{(M)}} = 0$ for such scatterers. The assessment of (23) and (24) reveals that α_m is the only parameter that might make $\frac{V_n^{(m)}}{U_n^{(M)}} = 0$ without forcing $\frac{U_n^{(m)}}{U_n^{(M)}} = 0$. By referring to (19), $\alpha_m = 0$ when $\varepsilon_m = -\frac{n}{n+1}\varepsilon_c^{(m)}$ or for the dominant mode $\varepsilon_m = -\frac{1}{2}\varepsilon_c^{(m)}$.

The special solution of $\varepsilon_m = -\frac{1}{2}\varepsilon_c$ can be further examined by considering a core-shell with ε_c as the core and ε_s as the shell in an ambient region of ε_a (the superscript m is omitted for convenience). If $\varepsilon_s = -\frac{1}{2}\varepsilon_c$, the equivalent core permittivity that the ambient region sees equals ε_c from (10), and if $\varepsilon_s = -\frac{1}{2}\varepsilon_a$, the equivalent ambient permittivity that the core sees is equal to ε_a from (15). This fact means that such an intervening layer in a nanoparticle structure does not affect the permittivities that the adjacent layers see through this layer regardless of its thickness as long as it can be considered a sub-wavelength particle.

Case 2. It is mentioned in the last paragraph of the previous section that the utilization of ε_a is limited by the fact that one should know ε_a for all layers that are after the m th layer. However, for some special values of ε_m and γ_m , β_m can be equal to unity. In fact (20) shows that if one starts from the outermost layer, and designs that layer such that $\beta_m = 1$ with respect to ε_a , the procedure can be continued toward the innermost layers up to the m th layer. The outcome of the procedure is that $\beta_m = 1$ for all layers after the m th layer, and (23), for instance, only depends on β_m^α . This condition can ease manipulation of the internal fields in each layer for a specific design.

In addition to the above-mentioned cases, the new formulation of the internal fields can facilitate the numerical evaluation of the fields. Although numerical evaluation is not in the perspective of this report, one special case might not elude one: if $\varepsilon_m = \frac{\varepsilon_c^{(m)}}{2(n+1)}$, one can obtain $\frac{\alpha_m}{n+1} = 1$. Even if $\frac{\alpha_m}{n+1} = 1$, $\frac{U_n^{(m)}}{U_n^{(M)}}$ cannot be equal to $\frac{V_n^{(m)}}{U_n^{(M)}}$ since it requires that $j_n(k_m r_{m-1}) = y_n(k_m r_{m-1})$, which is not valid for $k_m r_{m-1} \ll 1$. The use of the approximate expressions for the Bessel functions leads to $k_m r_{m-1} = \sqrt{2n+1}$, which is obviously greater than unity. This instance shows that the approximate formulae should be used with caution to get meaningful results.

6. Conclusion

In summary, this study extends the idea of equivalent core permittivity to the equivalent ambient permittivity, and uses both permittivities to reformulate the Mie coefficients for induced internal fields of a subwavelength multilayer spherical scatterer when it is impinged upon by a plane wave. The reformulation provides new insight on the internal field induction for such a scatterer.

Data availability statement

No new data were created or analysed in this study.

ORCID iD

Arash Nassajy  0009-0006-0154-0430

References

- [1] Shore R A 2015 Scattering of an electromagnetic linearly polarized plane wave by a multilayered sphere: obtaining a computational form of mie coefficients for the scattered field *IEEE Antennas Propag. Mag.* **57** 69–116
- [2] Aden A L and Kerker M 1951 Scattering of electromagnetic waves from two concentric spheres *J. Appl. Phys.* **22** 1242–6
- [3] Aden A 1951 Electromagnetic scattering from spheres with sizes comparable to the wavelength *J. Appl. Phys.* **22** 601–5
- [4] Toon O B and Ackerman T 1981 Algorithms for the calculation of scattering by stratified spheres *Appl. Opt.* **20** 3657–60
- [5] Bhandari R 1985 Scattering coefficients for a multilayered sphere: analytic expressions and algorithms *Appl. Opt.* **24** 1960–7
- [6] Zhang J 2025 A modified recursive transfer matrix algorithm for radiation and scattering computation of a multilayered sphere *J. Quant. Spectrosc. Radiat. Transfer* **338** 109401
- [7] Wu Z and Wang Y 1991 Electromagnetic scattering for multilayered sphere: recursive algorithms *Radio Sci.* **26** 1393–401
- [8] Johnson B 1996 Light scattering by a multilayer sphere *Appl. Opt.* **35** 3286–96
- [9] Kai L and Massoli P 1994 Scattering of electromagnetic-plane waves by radially inhomogeneous spheres: a finely stratified sphere model *Appl. Opt.* **33** 501–11
- [10] Wu Z S, Guo L X, Ren K F, Gouesbet G and Gréhan G 1997 Improved algorithm for electromagnetic scattering of plane waves and shaped beams by multilayered spheres *Appl. Opt.* **36** 5188–98
- [11] Yang W 2003 Improved recursive algorithm for light scattering by a multilayered sphere *Appl. Opt.* **42** 1710–20
- [12] Peña O and Pal U 2009 Scattering of electromagnetic radiation by a multilayered sphere *Comput. Phys. Commun.* **180** 2348–54
- [13] Ladutenko K, Pal U, Rivera A and Peña-Rodríguez O 2017 Mie calculation of electromagnetic near-field for a multilayered sphere *Comput. Phys. Commun.* **214** 225–30
- [14] Moroz A 2005 A recursive transfer-matrix solution for a dipole radiating inside and outside a stratified sphere *Ann. Phys., NY* **315** 352–418
- [15] Li R and Li B Q 2022 Efficient progressive algorithm for light scattering of a multilayered concentric nanoparticle *Appl. Opt.* **61** 10 556–66
- [16] Wait J R 1962 Electromagnetic scattering from a radially inhomogeneous sphere *Appl. Sci. Res. B* **10** 441–50
- [17] Sihvola A and Lindell I V 1988 Transmission line analogy for calculating the effective permittivity of mixtures with spherical multilayer scatterers *J. Electromagn. Waves Appl.* **2** 741–56

- [18] Sihvola A and Lindell I 1989 Polarizability and effective permittivity of layered and continuously inhomogeneous dielectric spheres *J. Electromagn. Waves Appl.* **3** 37–60
- [19] Tzarouchis D C and Sihvola A 2018 Polarizability of radially inhomogeneous subwavelength spheres *Phys. Rev. Appl.* **10** 054012
- [20] Alù A and Engheta N 2005 Polarizabilities and effective parameters for collections of spherical nanoparticles formed by pairs of concentric double-negative, single-negative, and/or double-positive metamaterial layers *J. Appl. Phys.* **97** 9
- [21] Alù A and Engheta N 2006 Erratum: polarizabilities and effective parameters for collections of spherical nanoparticles formed by pairs of concentric double-negative, single-negative, and/or double-positive metamaterial layers [J. Appl. Phys. 97, 094310 (2005)] *J. Appl. Phys.* **99** 6
- [22] Alù A and Engheta N 2005 Achieving transparency with plasmonic and metamaterial coatings *Phys. Rev. E Stat. Nonlin. Soft Matter Phys.* **72** 016623
- [23] Alù A and Engheta N 2006 Erratum: achieving transparency with plasmonic and metamaterial coatings [Phys. Rev. E, 72, 016623 (2005)] *Phys. Rev. E* **73** 019906
- [24] Tsitsas N L 2009 Direct and inverse dipole electromagnetic scattering by a piecewise homogeneous sphere *ZAMM Z. Angew. Math. Mech.* **89** 833–49
- [25] Kalogeropoulos A and Tsitsas N L 2023 Analytical algorithms for direct and inverse problems pertaining to the electromagnetic excitation of a layered medium by n dipoles *Math. Methods Appl. Sci.* **46** 16734–60
- [26] Nassajy A 2025 A recursive formula for the general scattering analysis of electrically small multilayer spherical scatterers *Next Res.* **2** 100843
- [27] Tzarouchis D C, Ylä-Oijala P and Sihvola A 2016 Unveiling the scattering behavior of small spheres *Phys. Rev. B* **94** 140301
- [28] Tzarouchis D C and Sihvola A 2018 General scattering characteristics of resonant core–shell spheres *IEEE Trans. Antennas Propag.* **66** 323–30
- [29] Tzarouchis D and Sihvola A 2018 Light scattering by a dielectric sphere: perspectives on the mie resonances *Appl. Sci.* **8** 184
- [30] Tzarouchis D C, Ylä-Oijala P and Sihvola A 2017 Resonant scattering characteristics of homogeneous dielectric sphere *IEEE Trans. Antennas Propag.* **65** 3184–91
- [31] Chen L, Ong C, Tan B and Deng C 1998 Effective permittivity of layered dielectric sphere composites *J. Mater. Sci.* **33** 5891–4
- [32] Zhang L, Shi Y and Liang C-H 2016 Achieving illusion and invisibility of inhomogeneous cylinders and spheres *J. Opt.* **18** 085101
- [33] Zhang L, Shi Y and Liang C-H 2016 Optimal illusion and invisibility of multilayered anisotropic cylinders and spheres *Opt. Express* **24** 23333–52
- [34] Stratton J A 2007 *Electromagnetic Theory* vol 33 (Wiley)
- [35] Balanis C A 2012 *Advanced Engineering Electromagnetics* (Wiley)
- [36] Hulst H C and van de Hulst H C 1981 *Light Scattering by Small Particles* (Courier Corporation)
- [37] Veselago V G 1968 The electrodynamics of substances with simultaneously negative values of ϵ and μ *Phys.-Usp.* **10** 509–14
- [38] Kalogeropoulos A and Tsitsas N L 2022 Electromagnetic interactions of dipole distributions with a stratified medium: power fluxes and scattering cross sections *Stud. Appl. Math.* **148** 1040–68